



Received 8 February 2022; revised 8 April 2022; accepted 23 April 2022. Date of publication 20 June 2022; date of current version 7 July 2022.

Digital Object Identifier 10.1109/JMW.2022.3171505

High-Sensitive Parity-Time Symmetric Oscillator in Coupled Transmission Lines With Nonlinear Gain

HAMIDREZA KAZEMI[®], ALIREZA NIKZAMIR[®], TAREK MEALY[®], AHMED ABDELSHAFY[®], AND FILIPPO CAPOLINO[®] (Fellow, IEEE)

(Invited Paper)

Department of Electrical Engineering and Computer Science, University of California, Irvine, CA 92697 USA

CORRESPONDING AUTHOR: Filippo Capolino (e-mail: f.capolino@uci.edu).

This work was supported in part by the National Science Foundation under Award NSF ECCS-1711975 and in part by Northrop Grumman.

ABSTRACT A scheme for generating oscillations based on an exceptional point of degeneracy (EPD) is proposed in two-coupled resonators made of two coupled transmission lines terminated on balanced gain and loss, exhibiting a double pole. The EPD is a point in the parameter space of the system at which two or more eigenmodes coalesce in both their eigenvalues (here, resonance frequencies) and eigenvectors. We show that a finite-length single transmission line terminated with gain and loss possesses no degeneracy point, whereas second-order EPDs are enabled in two finite-length coupled transmission lines (CTLs) terminated with balanced gain and loss. We demonstrate the conditions for EPDs to exist for three different termination configurations with balanced gain and loss, and show the eigenfrequency bifurcation at the EPD following the fractional power expansion series related to the Puiseux series. We study the oscillatory regime of operation assuming the gain element is nonlinear, and the extreme sensitivity of the degenerate self-oscillation frequency to perturbations and how it compares with the sensitivity of the linear-gain case. Finally, we show that the sensitivity of the EPD-CTL resonator is much higher than the one of a single-TL resonator. The very sensitive EPD based oscillator can be used as sensors when very small variations in a system shall be detected.

INDEX TERMS Coupled mode analysis, microwave oscillators, microwave sensors, resonators, sensitivity analysis.

I. INTRODUCTION

Oscillators are one of the essential components to generate radio frequency, microwave and optical signals. Typically, oscillators use a gain device through a positive feedback mechanism and a frequency selective circuit which generates a single frequency output. Conventional oscillators such as Van der Pol and voltage-controlled oscillators are among the most utilized oscillators at radio frequencies (RF) due to their simplicity of design and ease of fabrication [1], [2]. These oscillators are based on the LC-tank circuit and require a negative conductance for positive feedback obtained by simple circuit structures such as a cross-coupled pair [2]. A negative conductance can be also obtained from other circuit topologies such as Pierce, Colpitts, and Gunn diode waveguide

oscillators [2]–[6]. These kinds of oscillators are based on a single-pole operation, i.e., the system has one isolated pole that is rendered unstable, whereas, in this work, we propose a regime of oscillation based on a double pole that is obtained using a special second-order degeneracy discussed next.

Due to the importance and almost omnipresent use of oscillators in every RF and microwave system, finding new schemes for performing oscillator structures is an essential research avenue and novel principles of RF and microwave generation shall be continuously investigated [6]–[10]. Design principles of outed [11], [12], coupled [13], [14] and multi-mode [7] structures. This paper focuses on an oscillator concept based on an exceptional point of degeneracy (EPD) in a cavity made of two coupled transmission lines (CTLs);

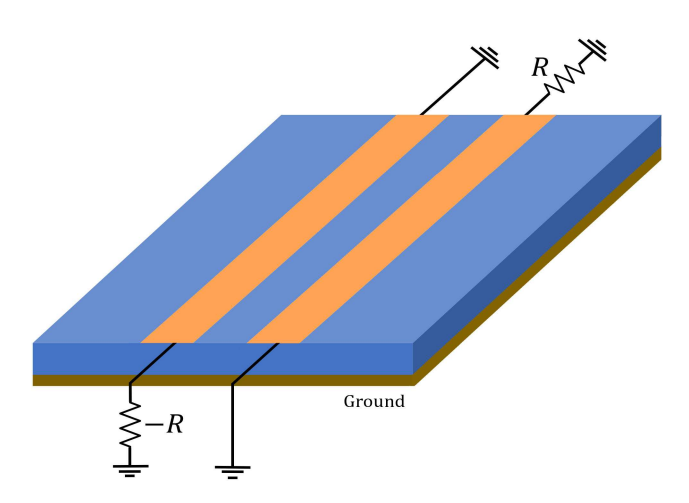


FIGURE 1. Two parallel coupled microstrip lines on a grounded dielectric substrate with terminations on a ground plane. This configuration exhibits the strong degeneracy condition called EPD.

an example is shown in Fig. 1, terminated on balanced gain and loss. As we will show, it has the particular feature that the resonance frequency is highly sensitive to a system's perturbation. The concept described here featuring an EPD can be potentially implemented in highly efficient oscillating arrays of antennas and highly sensitive sensor applications.

An EPD is a point in the parameter space of a system at which the system's eigenvectors, besides the eigenvalues, coalesce [15]–[18] (note that the term EP was already mentioned in Kato's book in 1966). The phenomenon of degeneracy of both eigenvalues and eigenvectors is a stronger degeneracy condition compared to the traditional degeneracy that often refers to only the degeneracy of two resonance frequencies, but does not necessarily imply the coalescence of the eigenvectors. Since the main feature of an EPD is the degeneracy in both eigenvectors and eigenvalues, we find it important to refer to it as a "degeneracy" [19], hence the inclusion of the "D" in the acronym EPD. The order of the degeneracy represents the number of the coalescing eigenmodes.

In recent years, EPDs have been commonly associated with the presence of gain and/or loss and often related to parity-time (PT)-symmetric systems where EPDs occur in the parameter space of a system described by its state's evolution in time [20]–[26] or in space [27]–[29]. The concept of EPDs has been applied to systems made of coupled resonators [20]–[24], [26], [30]–[32], and in systems of coupled modes in waveguides [27]–[29], [33]–[37], where the coalescence of eigenfrequencies and wavenumbers have been observed, respectively.

EPDs have been often found in systems with space or time periodicity (in the absence of gain and loss) supporting Floquet-Bloch waves such as photonic crystals and space periodic waveguides [27], [29], [33]–[35], [38], [39] and as time-periodic resonators [40]–[42].

In this paper, we present two interesting concepts: the double pole oscillator where the instability is related to a double pole instead of the usual one, and also an application of this concept as a very sensitive sensor. In particular, we study a system made of two distributed resonators, i.e., made of two coupled waveguides terminated on balanced gain and loss elements. It is important to distinguish between EPDs in systems made of coupled resonator (as in this paper) where the eigenvalues are the natural frequencies, and EPDs in waveguides where the eigenvalues are the wavenumbers. This paper deals with two coupled resonators made of two coupled waveguides of finite length, therefore the coalescing eigenvalues are two eigenfrequencies.

In the following, we first discuss the eigenfrequency of a "single pole" resonator made of finite-length transmission lines (TL) terminated on a gain and loss balance condition. Then, we investigate two CTLs terminated with balanced gain and loss following the PT-symmetry scheme and we show the existence of EPDs in such structures under different gain and loss configurations. Moreover, we characterize the performance of the CTL "double pole" oscillators operating at an EPD and show the transient behavior and their frequency response. We discuss the location of the double "poles" or "zeros" of the system and how they are sensitive to perturbations. Finally, we show the large resonance frequency shift due to system's perturbations and discuss how such shift is predicted by the Puiseux fractional power expansion related to the Puiseux series. Such large frequency shift is also observed from time-domain simulation results obtained by Keysight ADS circuit simulator using nonlinear gain [39], [43] representing active semiconductor components based on CMOS transistors or operational amplifiers. The proposed circuit and method can be used in ultra high-sensitive sensing applications. The EPD-based circuit has a double pole, which makes the oscillation frequency highly sensitive to any perturbation to the system, like changes in permittivity, load resistance, etc. Indeed, the high sensitivity could be a drawback when implementing an oscillator using the proposed concept because the oscillation frequency would be highly sensitive to any imperfection, however, because of this sensitivity feature can also be used to our advantage, the proposed circuit is a good candidate for being used in sensing applications. The concepts explained here can be generalized to even higher operating frequencies.

II. SINGLE TL OSCILLATOR

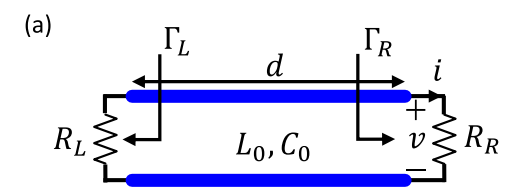
We consider a single finite-length TL terminated with a gain element (i.e., negative resistance) at one end and with a resistive load at the other end as shown in Fig. 2(a) where $Z_0 = \sqrt{L_0/C_0}$ is the characteristic impedance of the TL and d is its length. The resonance condition is

$$1 - \Gamma_L \Gamma_R e^{-j2\beta d} = 0, \tag{1}$$

where $\beta = \omega \sqrt{L_0 C_0}$ is the propagation constant, $\Gamma_L = (R_L - Z_0)/(R_L + Z_0)$ and $\Gamma_R = (R_R - Z_0)/(R_R + Z_0)$ are the reflection coefficients at the left and right ports, respectively $(R_L$ is assumed negative), and we implicitly adopt the $\exp(j\omega t)$ time convention. The complex-valued resonance frequency of such







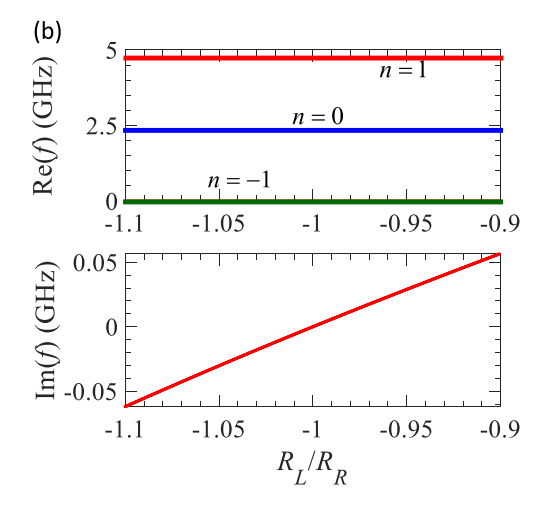


FIGURE 2. (a) Single finite-length TL terminated with R_L and R_R at its left and right ports, respectively. (b) Real and imaginary parts of the resonance frequency for different harmonics, calculated using (2). The complex resonance frequencies are calculated with the parameters of the structure set as $L_0=480\,\mathrm{nH}$, $C_0=57.9\,\mathrm{pF}$, $d=40.1\,\mathrm{mm}$, $R_R=50\,\Omega$ and varying R_L . There is no EPD.

a structure is derived from (1) as

$$f_n = \frac{1}{4\pi d\sqrt{L_0 C_0}} \left(\angle \Gamma_L + \angle \Gamma_R + 2n\pi - j \ln |\Gamma_L \Gamma_R| \right). \quad (2)$$

In general, for arbitrary values of R_L and R_R , the resonance frequency of such a structure is complex with a positive imaginary part when $|\Gamma_L \Gamma_R| < 1$, corresponding to decaying voltage and current; it has a negative imaginary part for $|\Gamma_L \Gamma_R| > 1$ corresponding to growing voltage and current in a lossless transmission line. In other words, for a nonzero imaginary part of the resonance frequency, an initial energy in the system will fully dissipate or will grow indefinitely. However, assuming $|\Gamma_L \Gamma_R| = 1$, the resonance frequency is purely real and such a condition corresponds to $R_L + R_R = 0$. Under this condition, we have a single TL where its left and right ports are terminated with balanced gain and loss loads, i.e., the two loads have the same magnitude with opposite signs (in other words, the resonator satisfies PT-symmetry). PT-symmetry is based on the combination of two operators: the "P" parity transformation to make spatial reflections $(x \to -x)$ and the "T" time-reversal transformation $(t \to -t)$, where x is the transverse coordinate and t is the time. In the phasor domain, the time-reversal operator "T" makes the imaginary unit $j \rightarrow -j$, hence loss goes into gain and vice versa. Therefore, since $\Gamma_L\Gamma_R = 1$, the structure has purely real resonance frequencies regardless of balanced gain and loss values. One may note that there exists no coalescence of the modes in such a

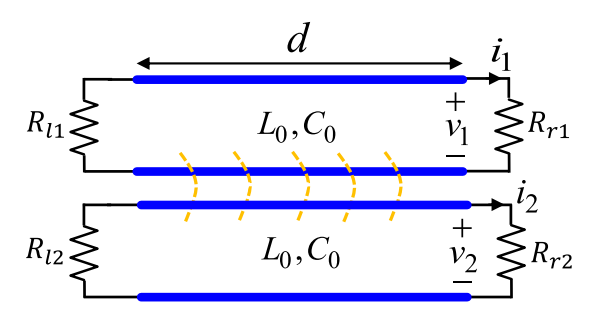


FIGURE 3. Two finite-length CTLs with terminations. The CTLs are both electrically and magnetically coupled. This configuration exhibits EPDs.

single TL with balanced gain and loss; thus, we do not observe any exceptional point. Fig. 2(b) shows the three lowest resonance frequencies of the single TL terminated with gain R_L and loss R_R for different values of R_L/R_R . The parameters are set as $L_0 = 480$ nH, $C_0 = 57.9$ pF, d = 40.15 mm, and $R_R = 49.88$ Ω . This plot shows that the single TL has a purely real oscillation frequency when gain and loss are balanced. In summary, this system supports independent resonance modes and cannot achieve exceptional degeneracy of modes required for the occurrence of exceptional points.

III. COUPLED TLS OSCILLATOR

Two coupled, lossless, and identical TLs with finite length are shown in Fig. 3, terminated with resistive loads R_{l1} and R_{l2} at their left ports, and resistive loads R_{r1} and R_{r2} at their right ports. This is a model of the coupled microstrip circuit in Fig. 1, as well as many others. The distributed (per-unit-length) inductance and capacitance of the lines when they are isolated are L_0 and C_0 , hence, the per unit length inductance and capacitance matrices of the coupled lines reads as [44], [45]

$$\underline{\mathbf{L}} = \begin{bmatrix} L_0 & L_m \\ L_m & L_0 \end{bmatrix}, \quad \underline{\mathbf{C}} = \begin{bmatrix} C_0 + C_m & -C_m \\ -C_m & C_0 + C_m \end{bmatrix}, \tag{3}$$

when the coupling between the lines is modeled by introducing a mutual per unit length inductance and capacitance L_m and C_m . Such a structure supports four different propagating modes with propagation constants $\pm k_e$ and $\pm k_o$ where (see Appendix A for derivation)

$$k_e = \omega/u_e, \quad k_o = \omega/u_o,$$
 (4)

and $u_e = 1/\sqrt{(L_0 + L_m)C_0}$ and $u_o = 1/\sqrt{(L_0 - L_m)(C_0 + 2C_m)}$ are the phase velocities of the even and odd modes.

Using the even and odd mode wavenumbers of the modes in the infinitely long CTL given in (4), we write the state vector $\Psi = [V_1, V_2, I_1, I_2]^T$ that describes the voltages and currents at any point z as the summation of four modes

$$\Psi(z) = \Psi_e^+ e^{-jk_e z} + \Psi_e^- e^{jk_e z} + \Psi_o^+ e^{-jk_o z} + \Psi_o^- e^{jk_o z},$$
 (5)

TABLE 1. Boundary Conditions for the Three Cases Shown in Fig. 4

Case I	Case II	Case III
$V_1(0) - R I_1(0) = 0$	$V_1(0) - R I_1(0) = 0$	
$V_2(0) = 0$	$V_2(0) = 0$	$V_2(0) + R I_1(0) = 0$
$V_1(d) - RI_1(d) = 0$		$V_1(d) = 0$
$V_2(d) = 0$	$V_2(d) - R I_2(d) = 0$	$V_2(d) = 0$

where the corresponding eigenvectors are

$$\Psi_{e}^{+} = V_{e}^{+} \begin{bmatrix} 1, & 1, & Y_{e}, & Y_{e} \end{bmatrix}^{T},
\Psi_{e}^{-} = V_{e}^{-} \begin{bmatrix} 1, & 1, & -Y_{e}, & -Y_{e} \end{bmatrix}^{T},
\Psi_{o}^{+} = V_{o}^{+} \begin{bmatrix} 1, & -1, & Y_{o}, & -Y_{o} \end{bmatrix}^{T},
\Psi_{o}^{-} = V_{o}^{-} \begin{bmatrix} 1, & -1, & -Y_{o}, & Y_{o} \end{bmatrix}^{T}.$$
(6)

Here, $Y_e = u_e C_0$ and $Y_o = u_o (C_0 + 2C_m)$ represent the characteristic admittances of the even and odd modes, respectively, and the superscript T denotes the transpose operation. Using the state vector in (5), in order to derive the resonance frequencies for the two finite-length CTLs shown in Fig. 3, we enforce the boundary conditions at the four ports of the structure (see Appendix B, Table 1). We obtain a homogeneous system of four linear equations as

$$\mathbf{A}(\omega)\mathbf{V} = \mathbf{0},\tag{7}$$

where $\mathbf{V} = [V_e^+, V_e^-, V_o^+, V_o^-]^{\mathrm{T}}$ represents the voltage amplitude vector, and (8), shown at the bottom of the page.

Free oscillation in such a structure occurs when there is a non-trivial solution of (7); therefore, oscillation frequencies are calculated as the roots of the vanishing determinant of $\underline{\mathbf{A}}$ as

$$\det(\mathbf{A}(\omega)) = 0. \tag{9}$$

At each resonance frequency ω_i , with i=1,2, derived from (9) (we only show frequencies with positive real part here), we find the vector kernel \mathbf{V}_i i=1,2 of the matrix $\underline{\mathbf{A}}(\omega_i)$ using the Gaussian elimination method. In other words, vectors \mathbf{V}_1 and \mathbf{V}_2 are the voltage amplitude vectors at the resonance frequencies ω_1 and ω_2 , respectively. Various choices could be made to measure the coalescence of the voltage amplitude vectors at the resonance frequencies, and here the Hermitian angle between the voltage amplitude vectors \mathbf{V}_1 and \mathbf{V}_2 is adopted and defined as [29], [46], [47]

$$\cos \theta = \frac{|\langle \mathbf{V}_1, \mathbf{V}_2 \rangle|}{\|\mathbf{V}_1\| \|\mathbf{V}_2\|}.$$

The $\cos\theta$ is defined via the inner product $\langle \mathbf{V}_1, \mathbf{V}_2 \rangle = \mathbf{V}_1^\dagger \mathbf{V}_2$, where the dagger symbol \dagger denotes the complex conjugate transpose operation, $|\cdot|$ represents the absolute value and $\|\mathbf{V}\| = \sqrt{\langle \mathbf{V}, \mathbf{V} \rangle}$ represents the norm of a complex vector. According to this definition, when $\sin\theta = 0$ the voltage amplitude vectors \mathbf{V}_1 and \mathbf{V}_2 coalesce, corresponding also to the coalescence of the two resonance frequencies ω_1 and ω_2 .

In this paper, we are interested in CTLs terminated on symmetrically balanced gain and loss, hence, in the following we consider three different values of R, -R, and 0 as loads in such a structure. Note that, different arrangement of these three load values at four distinct ports of the structure results in twelve sets of boundary conditions. However, since the structure is symmetric with respect to its ports, these twelve arrangements of loads shrink to only three distinct ones; shown in Fig. 4(a), (c) and (e). In the following, we analyze each particular structure separately and find the resonance frequency in two CTLs with balanced gain and loss varying the gain/loss value R in the absence of voltage generators. Moreover, we show the existence of EPD resonances, where resonance frequencies coalesce as well as the corresponding voltage vectors \mathbf{V}_1 and \mathbf{V}_2 .

In the following examples, the CTL is made of two TLs with parameters $L_0 = 480 \,\text{nH}$, $C_0 = 57.9 \,\text{pF}$, $d = 40.15 \,\text{mm}$, they are same as those we used for the single TL, but we now consider the coupling inductance $L_m = 367.4 \,\text{nH}$ and capacitance $C_m = 102.7 \,\text{pF}$ between the two TLs. As shown later on, a gain-resistance value of $R = 49.88 \,\Omega$ will lead to an EPD of order two.

A. CASE I: $R_{l1} = -R$, $R_{l2} = 0$, $R_{r1} = R$, $R_{r2} = 0$

In this scenario, shown in Fig. 4(a), we assume that the upper CTL is loaded with linear -R at the left port and a positive R at the right port; while the lower CTL is short circuited at both ports. The boundary conditions which describe this scenario are given in Appendix B and the system's eigenfrequencies are calculated from solving

$$\det(\underline{\mathbf{A}}(\omega)) = \cos(\omega d/u_e)\cos(\omega d/u_o) + H_1\sin(\omega d/u_e)\sin(\omega d/u_o) - 1 = 0, \quad (10)$$

where

$$H_1 = \frac{4 - R^2 \left(Y_e^2 + Y_o^2 \right)}{2R^2 Y_o Y_o}.$$
 (11)

The real and imaginary parts of the resonance frequencies (eigenfrequencies) are depicted in Fig. 4(b) for different values of balanced gain and loss R. The blue colored curve represents the two fundamental resonances and the red colored curve shows the next two higher resonances. It can be

$$\underline{\mathbf{A}}(\omega) = \begin{bmatrix} 1 + Y_e R_{l1} & 1 - Y_e R_{l1} & 1 + Y_o R_{l1} & 1 - Y_o R_{l1} \\ 1 + Y_e R_{l2} & 1 - Y_e R_{l2} & -1 - Y_o R_{l2} & -1 + Y_o R_{l2} \\ (1 - Y_e R_{r1}) e^{-j\omega d/u_e} & (1 + Y_e R_{r1}) e^{j\omega d/u_e} & (1 - Y_o R_{r1}) e^{-j\omega d/u_o} & (1 + Y_o R_{r1}) e^{j\omega d/u_o} \\ (1 - Y_e R_{r2}) e^{-j\omega d/u_e} & (1 + Y_e R_{r2}) e^{j\omega d/u_e} - (1 - Y_o R_{r2}) e^{-j\omega d/u_o} - (1 + Y_o R_{r2}) e^{j\omega d/u_o} \end{bmatrix}.$$
(8)





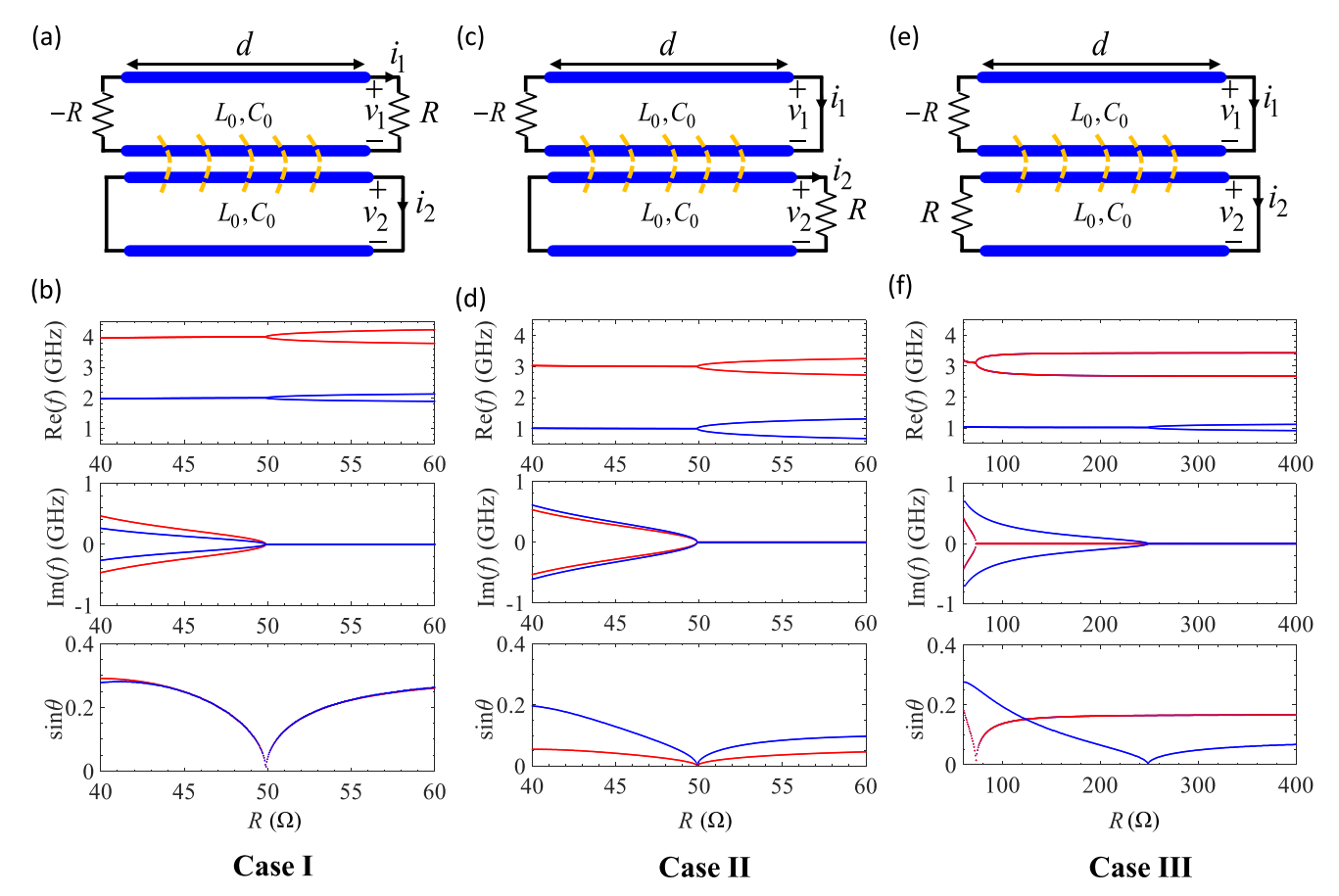


FIGURE 4. Three distinct cases of two coupled TLs termination and complex dispersion of the resonance frequencies. Blue lines show the two fundamental resonances and red lines represent the next two higher resonances. (a) Case I, showing the two coupled TLs where upper TL is terminated with linear gain -R and load R; and lower TL is shorted at both ports. (b) Plots of real and imaginary parts of resonance frequencies varying R for Case I depicted in (a). (c) Case II, two coupled TLs where upper TL is terminated with linear gain -R at the left port and it is shorted at the right port; and lower TL is shorted at the left port and it is terminated with load R at its right port. (d) Plots of real and imaginary parts of the resonance frequencies varying gain/load value R for Case II shown in (c). (e) Case III, two coupled TLs where upper TL is terminated with linear gain -R at the left port and it is shorted at the right port; lower TL is terminated with load R at the left port and it is shorted at its right port. (f) Plots of real and imaginary parts of the resonance frequencies varying gain/load value R for Case III shown in (e).

seen from these plots that the real and imaginary parts of the two resonance frequencies coalesce for a specific balanced gain/loss value R. The coalescence of the two eigenvalues is the result of the second-order EPD. In this scenario, the coalescence of the resonance frequencies for both the lower (blue line) and the higher (red line) resonances occur at the same balanced gain/loss value. Furthermore, the voltage amplitude vector \mathbf{V} is calculated for each of the two resonance frequencies (i.e., each eigenmode) using (7) and the bottom plot exhibits the coalescence angle between two vectors when varying R. The angle between the two voltage vectors vanishes where the resonance frequencies are identical which also indicates the coalescence of the polarization states, hence of the two modes and the occurrence of an EPD.

B. CASE II: $R_{l1} = -R$, $R_{l2} = 0$, $R_{r1} = 0$, $R_{r2} = R$

In the second scenario shown in Fig. 4(c), the upper CTL is connected to linear -R at the left port and shorted at the other port; and the lower CTL is shorted at the left port and

terminated with load R at the right one. Thus, enforcing the boundary conditions, the determinant in (9) is derived from

$$\det(\underline{\mathbf{A}}(\omega)) = \cos(\omega d/u_e)\cos(\omega d/u_o) + H_1\sin(\omega d/u_e)\sin(\omega d/u_o) + 1 = 0, \quad (12)$$

and the coefficient H_1 is given (11). Similar to Case I, real and imaginary parts of the resonance frequencies (eigenfrequencies) of the structure are calculated and plotted in Fig. 4(d) when varying R. The blue colored curves and the red colored curves represent the lowest and the next higher pairs of resonance frequencies, respectively. Assuming the same CTLs lengths as in the previous Case I, the fundamental resonance frequencies happen around twice the resonance frequencies of Case I. Moreover, the coalescence of the two resonances for both lowest and next higher pairs of frequencies occurs at the same balanced gain/loss value; this is observed also by the vanishing angle between the two coalescing voltage vectors when varying R, confirming the occurrence of the EPDs.

C. CASE III: $R_{l1} = -R$, $R_{l2} = R$, $R_{r1} = 0$, $R_{r2} = 0$

In the third scenario shown in Fig. 4(e), the upper CTL is terminated with linear -R at the left port and its right port is shorted. Moreover, the lower CTL is terminated with R at its left port and it is shorted at the right port. With this combination of terminations, the system's eigenfrequencies are found by satisfying

$$\det(\underline{\mathbf{A}}(\omega)) = \cos(\omega d/u_e)\cos(\omega d/u_o) + \frac{1}{R^2 Y_e Y_o} \sin(\omega d/u_e)\sin(\omega d/u_o) = 0. \quad (13)$$

The roots of the determinant represent the resonance frequencies of the system. The real and imaginary parts of the resonance frequencies (eigenfrequencies) are plotted in Fig. 4(f) for different values of the gain/loss value *R*. The real and imaginary parts of the pair of fundamental (lowest) and next higher resonance frequencies coalescence for different gain/loss values. The red colored curves show the pair of higher resonance frequencies, coalescence for a smaller value of gain/loss balance compared to the coalescence of the pair of fundamental frequencies (blue curves). Moreover, in this case the vanishing of the angle between the voltage vectors when varying *R*, demonstrates the coalescence of the pairs of voltage vectors, demonstrating the occurrence of the EPDs.

IV. CTLS OSCILLATOR CHARACTERISTICS

We show some important features of an oscillator based on the CTLs of Case II, namely, the transient time-domain behavior, frequency spectrum, and sensitivity to perturbations. The oscillator is studied using a cubic model (nonlinear) of the active component providing gain. The CTL parameters used here are the same as those used in the previous section. A value $R = 49.88 \,\Omega$ leads to an EPD of order two at a frequency of 1 GHz.

A. TRANSIENT BEHAVIOR AND FREQUENCY SPECTRUM

The time-domain (TD) response of the proposed CTLs oscillator as well as its frequency spectrum are depicted in Fig. 5 where the structure is terminated with balanced gain and loss satisfying the resonance condition in (12). The TD simulation result is obtained using the TD method implemented in the circuit simulator of Keysight ADS. The gain element is realized using a cubic model with an i-v curve described as

$$i = -g_m v + \alpha v^3, \tag{14}$$

shown in Fig. 5(a), where $-g_m$ is the negative slope of the i-v curve in the active resistance region and α is the third-order nonlinearity constant that models the saturation characteristic of the device. To realize a constant DC voltage-biased active device, we choose the turning point V_b of the i-v characteristics to be constant (when varying g_m) and equal to $V_b=1$ V under different biasing levels. The value of the saturation characteristic α determines the steady-state oscillation amplitude and in particular, we set $\alpha=g_m/(3V_b^2)$.

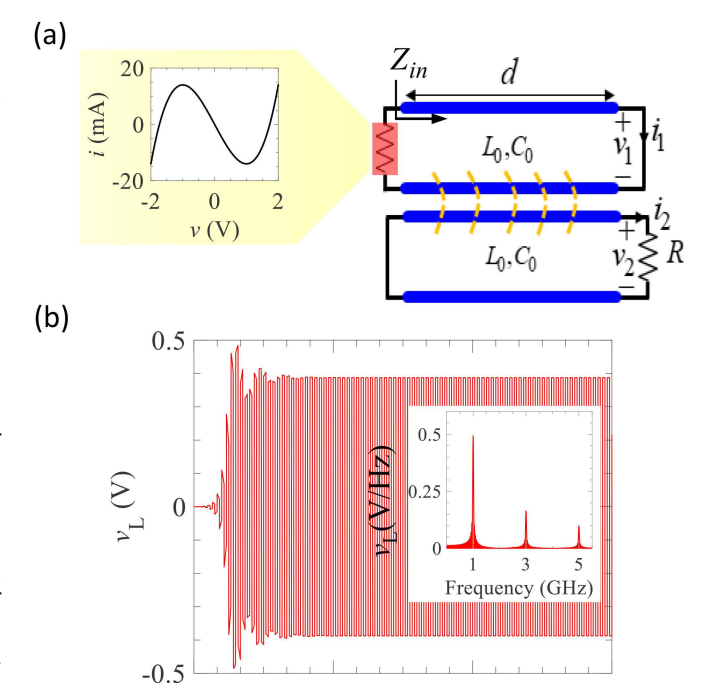


FIGURE 5. (a) The cubic model used as a realistic gain element where its i-v curve is shown in the inset. Parameters of the cubic model are set as gain $g_m=20.1$ mS, $\alpha=6.7$ mS and saturation voltage $V_b=1$ V. (b) Time-domain simulation result of the PT-symmetric oscillator shown in (a) and the frequency spectrum of the load voltage as the inset.

t (nsec)

30

60

90

Moreover, for simplicity we assume that the parasitic capacitance associated with the negative resistance device is negligible. In the shown TD results, the resistor is chosen to be $R = 49.88\Omega$, the g_m has been increased by 0.1% from its EPD gain-loss balanced value (in other words, the PT-symmetry is slightly perturbed), hence $g_m = 1.001/R$, in order to make the system unstable, hence to start and reach a stable oscillation. We use a voltage pulse at the right port of the first transmission line as the initial condition to start oscillations (alternatively, the simulation may have assumed the presence of noise to start oscillations). The frequency spectrum of the voltage at the load location is shown as an inset in Fig. 5(b), and it shows the fundamental frequency and harmonics of the oscillating voltage. The harmonics of the fundamental frequency are generated by the nonlinear nature of the gain element. An important observation is that the oscillation frequency mainly coincides with the fundamental EPD frequency of 1 GHz.

B. DOUBLE POLE BEHAVIOR AND HIGH SENSITIVITY TO PERTURBATIONS

In this subsection, we study the system in the frequency (phasor) domain to offer a different perspective of the special degeneracy discussed in this paper. The resonance frequencies of the system are here determined by using the impedance resonance method, and we show the relation between the EPD and the occurrence of double solutions (double zeros).





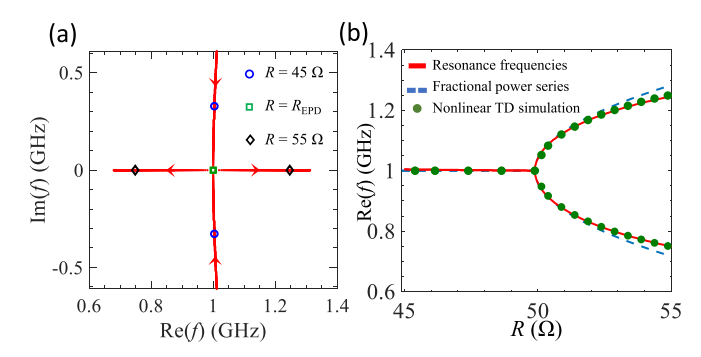


FIGURE 6. (a) Root locus of two frequency zeros of $Z_{in}(2\pi f)-R$ showing the fundamental pairs of resonance frequencies of the CTLs in Case II, varying both the linear negative and positive values of R. (b) Resonance frequencies obtained from solving (9) (red line), and from the first-order fractional power expansion series expansion (dashed blue line), when varying both the linear gain and resistance R. Results accounting for the nonlinear cubic model of the gain elements (14) using the time-domain circuit simulator by ADS Keysight are shown by green dots, where $g_m = 1.001/R$ has been increased by 0.1% from its loss balanced value.

With reference to the Case II structure in Fig. 6(a), the resonance condition imposed by the vanishing of the total series impedance implies that

$$Z_{in}(\omega) - R = \frac{\det\left[\underline{\mathbf{A}}(\omega)\right]}{P(\omega)} = 0, \tag{15}$$

where $P(\omega)$ is

$$P(\omega) = R\left(Y_0^2 + Y_e^2\right) \sin\left(\frac{\omega d}{u_e}\right) \sin\left(\frac{\omega d}{u_0}\right)$$
$$-2RY_e Y_o \left(1 + \cos\left(\frac{\omega d}{u_e}\right) \cos\left(\frac{\omega d}{u_0}\right)\right)$$
$$-2j\left(Y_e \cos\left(\frac{\omega d}{u_e}\right) \sin\left(\frac{\omega d}{u_0}\right)$$
$$+Y_o \cos\left(\frac{\omega d}{u_0}\right) \sin\left(\frac{\omega d}{u_e}\right)\right), \tag{16}$$

and -R is the gain element, assumed linear in this subsection. Here, $Z_{in}(\omega)$ is the input impedance of the CTLs seen from the upper left port when a load resistor R is connected to the bottom right port, shown in Fig. 5(a). The input impedance is obtained using the transfer matrix $\underline{\mathbf{T}} = \exp(-j\omega \underline{\mathbf{M}}d)$ of a CTL of length d, where is the waveguide system matrix M is defined in Appendix A, and assuming the upper CTL is shorted at the right port, and the lower CTL is shorted at the left port, as discussed in Appendix B. The series total impedance $Z_{in}(\omega) - R$ has the same ω -zeros as $\det[\underline{\mathbf{A}}(\omega)]$. Note that $\omega(R)$ and $-\omega^*(R)$ are both solutions of (15). In Fig. 6(a), we plot the zeros with $Re(\omega) > 0$ of $Z_{in}(\omega) - R$ for varying R, in the complex frequency plane (there are other zeros, but we plot only those relative to the fundamental pair of frequencies). The trajectory of the resonance frequencies ω for the two modes with $Re(\omega) > 0$ are plotted with increasing resistance R from 40Ω to 60Ω . The double zero at ω_{EPD} occurs at $R_{EPD} = 49.88 \,\Omega$, where the two curves meet.

Therefore, when $R = R_{EPD} = 49.88 \,\Omega$, for frequencies close to the EPD one can write $Z_{in}(\omega) - R \propto (\omega - \omega_{EPD})^2$ and the resonance condition becomes $(\omega - \omega_{EPD})^2 = 0$, which shows the double (degenerate) resonance. From this interesting property one can infer that if a perturbation is applied to the circuit so it is not anymore at its EPD, the variation of the resonance frequency follows a square root behavior, which is the key to high sensitivity. For resistances such that $R > R_{EPD}$, the two resonance frequencies are purely real, despite the presence of balanced losses and gain. Instead, for $R < R_{EPD}$, the two resonance frequencies are complex conjugate, as shown in Fig. 6.

V. OSCILLATION FREQUENCY HIGHLY SENSITIVE TO PERTURBATIONS

It is known that in systems operating at EPDs some quantities (like eigenvalues and eigenvectors) are extremely sensitive to perturbation of system parameters. In particular, a small perturbation Δ_X of a system parameter X results in a tremendous change in the state of the system [25], [41], [48]. By applying a perturbation Δ_X as

$$\Delta_{X} = \frac{X - X_{EPD}}{X_{EPD}},\tag{17}$$

where X is the perturbed component's value, and X_{EPD} is the unperturbed value that provides the EPD condition, the matrix $\underline{\mathbf{A}}(\Delta_{\mathrm{X}})$ is perturbed. In the CTLs structure with balanced gain and loss, the two degenerate resonance frequencies (they are the eigenvalues) change due to a small perturbation Δ_{X} , resulting in two distinct resonance frequencies, following the behavior predicted by the fractional power expansion series. The two perturbed angular eigenfrequencies $\omega_i(\Delta_{\mathrm{X}})$, with i=1,2, are estimated by using the fractional power expansion series around a second-order EPD given by

$$\omega_i (\Delta_{\rm X}) \simeq \omega_{EPD} + (-1)^i \alpha_1 \sqrt{\Delta_{\rm X}} + \alpha_2 \Delta_{\rm X}.$$
 (18)

Following the steps in Appendix C and [49], [50], we calculate the coefficients as

$$\alpha_1 = \sqrt{-\frac{\frac{\partial H(\Delta_X, \omega)}{\partial \Delta_X}}{\frac{1}{2!} \frac{\partial^2 H(\Delta_X, \omega)}{\partial \omega^2}}},$$
(19)

$$\alpha_2 = -\frac{\alpha_1^3 \frac{1}{3!} \frac{\partial^3 H(\Delta_X, \omega)}{\partial \omega^3} + \alpha_1 \frac{\partial^2 H(\Delta_X, \omega)}{\partial \omega \partial \Delta_X}}{\alpha_1 \frac{\partial^2 H(\Delta_X, \omega)}{\partial \omega^2}}, \quad (20)$$

where $H(\Delta_X, \omega) = \det[\underline{\mathbf{A}}(\Delta_X, \omega)]$ and its derivatives are evaluated at the EPD, i.e., at $\Delta_X = 0$ and $\omega = \omega_{EPD}$. This fractional power expansion provides a good approximation of the perturbed eigenfrequencies as demonstrated in the following.

We consider the CTLs in Case II shown in Fig. 4(c), with an EPD resonance when $R = R_{EPD}$, and we assume the same parameter values given in Sec. III-B. We apply a small perturbation in both linear gain and resistance as $R = R_{EPD}(1 + \Delta_R)$. The calculated coefficient $\alpha_1 = 5.56 \times 10^9$ rad/s is purely

real and Fig. 6(b) illustrates the separation between the two resonance frequencies varying the perturbation Δ_R .

The result in Fig. 6(b) demonstrates that for a small perturbation $-0.1 < \Delta_R < 0.1$ of both the positive and negative resistive terminations, the resonance frequency f is significantly changed for positive resistive changes $\Delta_R > 0$, where the real part of the resonance frequency follows the square root behavior. The square root behavior shows the exceptional sensitivity of the proposed system operating at an EPD, which can be used to conceive a new class of very sensitive sensors. For positive values Δ_R , the structure shows two real resonance frequencies. Fig. 6(b) exhibits also the structure's sensitivity due to the fractional power expansion series limited to its first order, displayed by a dashed line. Moreover, green dots show results using the nonlinear cubic model for gain: the frequencies are calculated from the Fourier transform of the time-domain circuit simulator implemented in Keysight ADS after reaching saturation, using the nonlinear cubic model for the gain in (14) where $g_m = 1.001/R$, i.e., has been increased by 0.1% from its loss balanced value. We use a voltage pulse at the right port of the first transmission line as the initial condition to start oscillations. For both resistance-gain perturbations with $R > R_{EPD}$, the circuit oscillates at two distinct resonance frequencies (green dots). This latter result demonstrates the ultra sensitive frequency of oscillation (green dots) of the oscillator when used in a sensor scheme. The fast Fourier transform is calculated from 500 MHz to 1.5 GHz using 10⁶ signal samples in the time window from 200 ns to 1 μ s.

A. SENSITIVITY TO VARIATIONS OF THE LOAD RESISTANCE R ONLY

This section discusses how sensitive the circuit is to the perturbation of only the passive resistance (i.e., the one on the lossy side). This perturbation could be the one happening in a sensor based on resistivity changes. By breaking PT-symmetry and perturbing just the lossy side resistance as $R = R_{EPD}(1 +$ $\Delta_{\rm R}$) from its EPD value R_{EPD} , while the (linear) gain component is kept fixed to $-R_{EPD}$, the circuit shows a large shift of the resonance frequencies for positive resistive changes $\Delta_{\rm R} > 0$, where the real part of the resonance frequency follows the square root behavior as shown in Fig. 7(a). This perturbation brings the system away from the PT-symmetry condition and the system becomes unstable demonstrated by the fact that shifted frequencies have an imaginary part with a negative sign, for either sign of Δ_R as shown in Fig. 7(b). The solid-red line shows the resonance frequency evaluation by solving (9), the dashed-blue line represents the two eigenfrequencies estimated by the fractional power expansion series truncated to its second order. The coefficients in (19) and (20) are calculated as $\alpha_1 = 3.95 \times 10^9 + j3.91 \times 10^8 \text{ rad/s}$ and $\alpha_2 = -9.40 \times 10^7 - j2.61 \times 10^9 \text{ rad/s}$, they are complex, which means that for all values of small loss resistance changes, the two eigenfrequencies are complex valued and the system is unstable, for either $\Delta_R < 0$, (i.e., $R < R_{EPD}$) or $\Delta_R > 0$ (i.e., $R > R_{EPD}$). For $\Delta_R > 0$, the bifurcation of $Re(\omega)$ is more significant than for $\Delta_R < 0$, thus, the circuit is

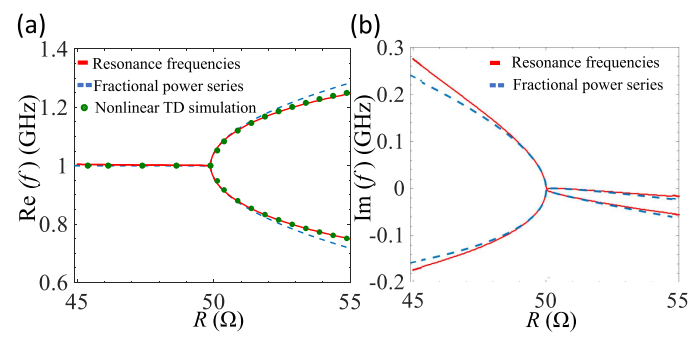


FIGURE 7. (a) Real part and (b) imaginary part of the eigenfrequencies, when varying only the load resistance and the gain is $-R_{EPD}$. The red-solid line represents the resonance frequencies obtained by solving (9), using linear model of the gain. The dashed-blue line represents the eigenfrequencies estimated using the fractional power expansion series up to the second order, using linear model of the gain. The green dots represent the frequencies obtained by applying the Fourier transform to the TD results using the nonlinear cubic model of the gain elements (14) where $g_m = 1.001/R$.

more sensitive to positive changes of Δ_R , corresponding to a larger value of $\text{Re}(\omega)$ than $\text{Im}(\omega)$. To have approximately the same frequency shift for either positive or negative relative perturbations Δ_R , one should design an EPD where the real and imaginary parts of α_1 are approximately equal. Moreover, the green dots show the frequencies calculated when using the nonlinear gain in (14), where g_m has been increased by 0.1% than the EPD value, hence $g_m = 1.001/R_{EPD}$. The result is obtained by applying the Fourier transform to the TD signal after reaching saturation evaluated using the circuit simulator implemented in Keysight ADS, using the same initial condition as in the last section. For different loss resistance perturbations, the circuit oscillates at two resonance frequencies, shown in green dots. This latter result demonstrates the high sensitivity of the frequencies of oscillation (green dots) when used in a sensor scheme. This configuration where the loss resistance is changing is useful for sensors like a moister detector, strain gauge, thermistor, etc. The frequency domain spectrum is calculated from 500 MHz to 1.5 GHz using 10⁶ signal samples in the time window from 200 ns to 1 μ s.

B. SENSITIVITY TO THE PER-UNIT-LENGTH CAPACITANCE C₀

The oscillator scheme described in this paper can be used as a distributed capacitance sensor, i.e., for sensing perturbations of the per-unit-length capacitance C_0 of both the CTLs as shown in Fig. 8. In this setup, the system is very sensitive to a change in permittivity in the materials (above or below) surrounding the CTLs. Assuming that the perturbation Δ_{C_0} is applied to the per unit length self capacitance of the CTLs C_0 , the perturbed C is expressed as $C = (1 + \Delta_{C_0})C_0$. In this scheme, the oscillation frequency is sensitive to negative changes of the per-unit-length capacitance $\Delta_{C_0} < 0$ where the real part of the resonance frequency follows the square root behavior. The active gain element is assumed to be the





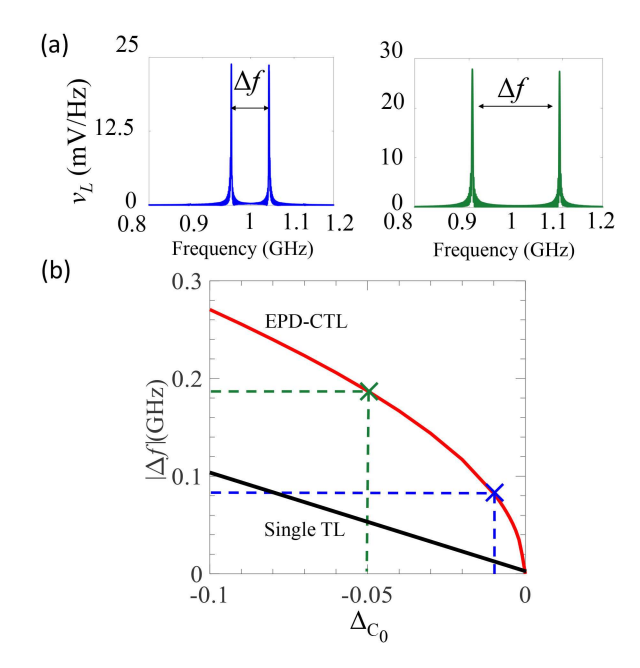


FIGURE 8. (a) Frequency spectrum of the load voltage obtained from the Fourier transform of the time-domain simulation result using the nonlinear cubic model of the gain elements (14) where $g_m=1.001/R_{EP,D}$. We perturb the per-unit-length capacitance as $\Delta_{C_0}=-1\%$ (blue line) and $\Delta_{C_0}=-5\%$ (green line). The system shows two oscillation frequencies and the separation depends on the perturbation. (b) Separation between the two oscillation frequencies varying Δ_{C_0} based on the EPD-CTL structure with nonlinear gain (red line). For comparison we also show the shift of the eigenfrequency of the resonator made of a single TL varying Δ_{C_0} (black line). The EPD-CTL shows much higher sensitiviy to a perturbation.

nonlinear cubic model in (14), where $g_m = 1.001/R_{EPD}$ has been increased by 0.1% from its EPD gain-loss balanced value $1/R_{EPD}$. Using a voltage pulse at the right port of the first transmission line as the initial condition the circuit starts to oscillate.

Fig. 8(a) shows the TD simulation result using Keysight ADS by using the cubic model for the gain in (14) of the perturbed circuit with $\Delta_{C_0} = -5\%$ (green color) and $\Delta_{C_0} =$ -1% (blue color). By perturbing C_0 , the circuit oscillates at two resonance frequencies as seen in the frequency spectrum of the load voltage in the inset, calculated from 500 MHz to 1.5 GHz using 10⁶ signal samples in the time window of 200 ns to 1 μ s. The two oscillation frequencies shift further away from each other when more perturbation is applied to C_0 . The difference between the two frequencies Δf is shown in Fig. 8(b) for negative values of Δ_{C_0} , obtained from TD simulations using nonlinear gain, and the square root-like behavior shows the high sensitivity to perturbations of C_0 . For instance, when C_0 is perturbed by -1% from its EPD value, the CTL shows the two real resonance frequencies at 959 MHz and 1.04 GHz, associated to a $\Delta f/f_{EPD} = 8.3\%$. Also, when C_0 is perturbed by -5% from its EPD value, the CTL shows the two real resonance frequencies at 906 MHz and 1.09 GHz, associated to a $\Delta f/f_{EPD} = 19\%$. In conclusion, when there is a small perturbation in the per-unit-length capacitance, the oscillation frequencies shift dramatically so the proposed circuit has a promising use as a scheme for high-sensitive sensors. To better understand how the EPD-based sensor improves the sensitivity compared to a conventional resonator, we compare its sensitivity to the one of single TL terminated with a short circuit on both sides without adding gain or loss. The lowest resonance condition for such single TL is $\beta d = \pi$, which corresponds to the resonance frequency $f = 1/(2d\sqrt{L_0C_0})$. By perturbing the per-unit length capacitance of the TL, C_0 , the resonance frequency is shifted by $\Delta f = -\Delta_{C_0}/(4d\sqrt{L_0C_0})$. In Fig. 8(b), we show a comparison between the shift of resonance frequency due to perturbations in C_0 for two cases: (i) the EPD-CTL (solid red line) and (ii) the single TL (solid black line). This figure shows that the sensitivity of the EPD-CTL structure with nonlinear gain (solid red line) is much higher (it follows a square-root-like behavior) than the one of the conventional TL without EPD (solid black line).

VI. CONCLUSION

We have shown the existence of a second-order EPD in two coupled resonators made of a pair of finite-length CTLs, terminated with balanced gain and loss satisfying different configurations of PT-symmetry. The degenerate eigenfrequencies are highly sensitive to perturbations of the system. We have also provided an alternative view of second-order EPD of the system observing the occurrence of a "double pole" and that the CTL oscillator oscillates at that double-pole frequency also when gain is nonlinear. We have analyzed three different scenarios to perturb the system. First, by perturbing both gain and loss together (PT-symmetry is slightly broken by putting gain 0.1% higher than the balanced loss value, to start oscillations), then by perturbing the loss resistance while the gain is kept constant and equal to the EPD value, and finally by perturbing the per-unit-length capacitance of both the TLs: all the three cases lead to large values of resonance frequency shifts and consequently to shifts of the self-oscillation frequencies. We have shown that the circuit's eigenfrequencies are exceedingly sensitive to a perturbation of the circuit components, and this may have significant implications in sensing technology and RF sensors. Note that however the system needs to work at, or very close to, the EPD to obtain the square root sensitivity. While any imperfection in manufacturing leads to a shift from the EPD, a fine-tuning process is required to configure the system at the EPD to be ready to exhibit the square root sensitivity to perturbations. Finally, we have demonstrated that the sensitivity of the EPD-based CTL oscillator is much higher than the one of a conventional resonator made of a single TL not working at an EPD.

APPENDIX A PROPAGATING MODES OF CTLS

Using the per-unit-length inductance $\underline{\mathbf{L}}$ and capacitance $\underline{\mathbf{C}}$ matrices, the telegrapher's equations for the coupled TLs are given by [27]

$$\frac{d}{dz}\psi = -j\underline{\mathbf{M}}\psi,\tag{A1}$$

where $\psi(z) = [V_1, V_2, I_1, I_2]^{\text{T}}$ is the state vector of the system representing voltages and currents along the two CTLs, and the system matrix **M** is obtained as

$$\underline{\mathbf{M}} = \begin{bmatrix} \underline{\mathbf{0}} & \omega \underline{\mathbf{L}} \\ \omega \underline{\mathbf{C}} & \underline{\mathbf{0}} \end{bmatrix}. \tag{A2}$$

Let us assume a time and space convention of the state vector as $\psi(z) \propto e^{-jkz}$, where ω is the angular frequency, and k is the wavenumber of a mode in the CTLs. Hence, four different propagating modes of the CTLs system are obtained by finding the roots (either in k or ω) of the characteristic equation of the system described in (A1) as

$$\det(\underline{\mathbf{M}} - k\underline{\mathbf{I}}) = k^4 - \omega^2 (u_e^{-2} + u_o^{-2})k^2$$
$$+ \omega^4 u_o^{-2} u_o^{-2} = 0. \tag{A3}$$

The *k* roots of the (A3) are the wavenumber of the even and odd modes propagating in the CTLs.

Solution of (A1), with a certain boundary condition $\psi(z_0) = \psi_0$ at a certain coordinate z_0 inside a uniform CTL segment, is found by representing the state vector solution at a coordinate z_1 using

$$\psi(z_1) = \mathbf{T}(z_1, z_0)\psi(z_0), \tag{A4}$$

where $\underline{\mathbf{T}}(z_1, z_0)$ is the transfer matrix which translates the state vector $\boldsymbol{\psi}(z)$ between two points z_0 and z_1 along the z-axis. For a uniform segment of two CTLs with length d, the transfer matrix is easily calculated as

$$\underline{\mathbf{T}} = \exp(-j\underline{\mathbf{M}}d). \tag{A5}$$

Using the obtained transfer matrix and assuming the resistor R is connected to the lower right port, the input impedance seen from the upper left port in Fig. 5(a) is

$$Z_{in} = -\frac{T_{13}T_{24} - T_{14}T_{23} - RT_{13}T_{44} + RT_{14}T_{43}}{T_{11}T_{24} - T_{14}T_{21} - RT_{11}T_{44} + RT_{14}T_{41}}.$$
 (A6)

APPENDIX B COUPLED TLS BOUNDARY CONDITIONS

We express the general boundary conditions for the two CTLs shown in Fig. 3 using the KVL at the four ports of the CTLs as

$$V_1(0) + R_{I1} I_1(0) = 0$$

$$V_2(0) + R_{I2} I_2(0) = 0$$

$$V_1(d) - R_{r1} I_1(d) = 0$$

$$V_2(d) - R_{r2} I_2(d) = 0$$
(B1)

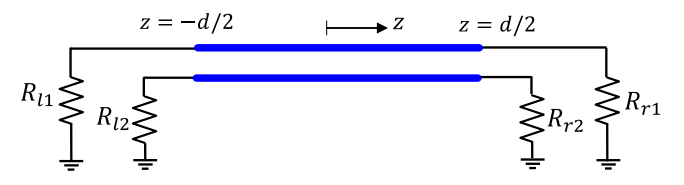


FIGURE 9. Shifting the *z*-axis to the middle of the transmission line to find the new **A**.

Therefore, applying the boundary conditions to (B1) which describe the three different cases shown in Fig. 4 leads to

Based on these boundary conditions, we find the determinant of the matrix $\underline{\mathbf{A}}(\omega)$ in (10), (12), and (13), and consequently the resonance frequencies for the three cases.

APPENDIX C

USING PUISEUX SERIES TO CALCULATE THE SENSITIVITY TO SYSTEM'S PERTURBATIONS

In this Appendix, the z-axis origin is assumed to be at the center of the CTL for convenience, and by applying the boundary conditions at z = -d/2 and z = d/2 shown in Fig. 9, the $\underline{\mathbf{A}}$ matrix reads (C1), shown at the bottom of the page.

The goal is to provide an analytical expression for the perturbed eigenfrequencies of the system when a small perturbation Δ_X is applied to one of its parameters or components without starting from an eigenvalue problem. The eigenfrequencies are given by solving $H(\Delta_X, \omega) \triangleq \det[\underline{\mathbf{A}}(\Delta_X, \omega)] = 0$ for ω . Close to the EPD angular frequency ω_{EPD} , the matrix $\mathbf{A}(\Delta_X, \omega)$ is expanded as

$$\underline{\mathbf{A}}(\Delta_{\mathbf{X}}, \omega) = \underline{\mathbf{A}}(\Delta_{\mathbf{X}}, \omega_{EPD}) + \frac{d\underline{\mathbf{A}}(\Delta_{\mathbf{X}}, \omega)}{d\omega}|_{\omega_{EPD}}(\omega - \omega_{EPD}) + \underline{\mathbf{O}}, \quad (C2)$$

where $\underline{\mathbf{O}}(\Delta_{\mathbf{X}}, \omega)$ defines higher order terms, i.e., terms that vanish at least as $(\omega - \omega_{EPD})^2$, where ω_{EPD} is the solution of $\det[\underline{\mathbf{A}}(\Delta_{\mathbf{X}}=0,\omega)]=0$. In order to apply the Puiseux series to find the perturbation of the eigenfrequencies for a small $\Delta_{\mathbf{X}}$, we rewrite the system equation $\underline{\mathbf{A}}(\Delta_{\mathbf{X}},\omega)\mathbf{V}=0$ in an eigenvalue problem form, e.g., as $(\underline{\mathbf{B}}-\omega\underline{\mathbf{I}})\mathbf{V}=0$, assuming that $\omega\approx\omega_{EPD}$, where $\underline{\mathbf{I}}$ is the 4×4 identity matrix. This can be achieved by left multiplying (C2) by $\underline{\mathbf{D}}(\Delta_{\mathbf{X}})\equiv -(\frac{d\underline{\mathbf{A}}(\Delta_{\mathbf{X}},\omega)}{d\omega}|_{\omega_{EPD}})^{-1}$. It is convenient to define

$$\mathbf{B}(\Delta_{\mathbf{X}}) = \omega_{EPD}\mathbf{I} + \mathbf{D}(\Delta_{\mathbf{X}})\mathbf{A}(\Delta_{\mathbf{X}}, \omega_{EPD}), \qquad (C3)$$

where $\underline{\mathbf{B}}$ depends only on the perturbation Δ_X , and not on ω . This procedure leads to

$$\underline{\mathbf{B}}(\Delta_{\mathbf{X}}) - \omega \underline{\mathbf{I}} = \underline{\mathbf{D}}(\Delta_{\mathbf{X}})\underline{\mathbf{A}}(\Delta_{\mathbf{X}}, \omega) + \underline{\mathbf{O}}_{\mathbf{B}}, \quad (C4)$$

$$\underline{\mathbf{A}}(\omega) = \begin{bmatrix} (1 + Y_e R_{l1}) e^{+j\omega d/(2u_e)} & (1 - Y_e R_{l1}) e^{-j\omega d/(2u_e)} & (1 + Y_o R_{l1}) e^{j\omega d/(2u_o)} & (1 - Y_o R_{l1}) e^{-j\omega d/(2u_o)} \\ (1 + Y_e R_{l2}) e^{+j\omega d/(2u_e)} & (1 - Y_e R_{l2}) e^{-j\omega d/(2u_e)} & (-1 - Y_o R_{l2}) e^{j\omega d/(2u_o)} & (-1 + Y_o R_{l2}) e^{-j\omega d/(2u_o)} \\ (1 - Y_e R_{r1}) e^{-j\omega d/(2u_e)} & (1 + Y_e R_{r1}) e^{j\omega d/(2u_e)} & (1 - Y_o R_{r1}) e^{-j\omega d/(2u_o)} & (1 + Y_o R_{r1}) e^{j\omega d/(2u_o)} \\ (1 - Y_e R_{r2}) e^{-j\omega d/(2u_e)} & (1 + Y_e R_{r2}) e^{j\omega d/(2u_e)} & -(1 - Y_o R_{r2}) e^{-j\omega d/(2u_o)} & -(1 + Y_o R_{r2}) e^{j\omega d/(2u_o)} \end{bmatrix}$$
(C1)





where $\underline{\mathbf{O}}_B = -\underline{\mathbf{D}}\underline{\mathbf{O}}$ is a term that vanishes at least as $(\omega - \omega_{EPD})^2$. Since from (7) we know that at each eigenfrequency one has $\underline{\mathbf{A}}(\Delta_X, \omega_i)\mathbf{V} = 0$, at those eigenfrequencies we have

$$(\underline{\mathbf{B}} - \omega_i \underline{\mathbf{I}}) \mathbf{V} = \underline{\mathbf{D}} \underline{\mathbf{A}} \mathbf{V} + \underline{\mathbf{O}}_R \mathbf{V} = \underline{\mathbf{O}}_R \mathbf{V} \approx 0.$$
 (C5)

Therefore, the terms of this equation tend to zero as $\omega_i \rightarrow \omega_{EPD}$, which means that the angular frequencies that satisfy $(\underline{\bf B} - \omega \underline{\bf I}) {\bf V} = 0$ and $\underline{\bf A} {\bf V} = 0$ are approximately the same, for any Δ_X , when they are very close to ω_{EPD} . Furthermore, when $\Delta_X = 0$, the eigenvalue of $(\underline{\bf B} - \omega \underline{\bf I}) {\bf V} = 0$, coincides with the ω -solution of $\underline{\bf A} {\bf V} = 0$. A more precise procedure should show also the higher order terms when discussing the approximation. We now use the Puiseux series expansion [50] to estimate the perturbed eigenvalues of $(\underline{\bf B} - \omega \underline{\bf I}) {\bf V} = 0$ when a perturbation Δ_X is applied to the system. The first-order Puiseux series expansion yields

$$\omega_i(\Delta_{\mathbf{X}}) \simeq \omega_{EPD} + (-1)^i \alpha_1 \sqrt{\Delta_{\mathbf{X}}},$$
 (C6)

which describes the perturbation of the two eigenvalues (i = 1, 2) when a small relative perturbation Δ_X of a system's parameter near its EPD value $\Delta_X = 0$ occurs. The series coefficients are calculated using the explicit recursive formulas given in [50] pertaining to the eigenvalue problem $(\underline{\mathbf{B}} - \omega \underline{\mathbf{I}})\mathbf{V} = 0$. Thus, to find α_1 we have to find the derivatives of $H_B(\Delta_X, \omega) \triangleq \det(\underline{\mathbf{B}} - \omega \underline{\mathbf{I}})$ with respect to Δ_X and ω at the EPD point as

$$\alpha_1 = \sqrt{-\frac{\frac{dH_B(\Delta_X,\omega)}{d\Delta_X}}{\frac{1}{2!}\frac{d^2H_B(\Delta_X,\omega)}{d\omega^2}}}|_{\omega_{EPD}, X_{EPD}}.$$
 (C7)

Using (C4), the relation between H_B and $H(\Delta_X, \omega) \triangleq \det \underline{\mathbf{A}}(\Delta_X, \omega)$ is found to be

$$H_B(\Delta_X, \omega) \approx \det \mathbf{D}(\Delta_X) H(\Delta_X, \omega).$$
 (C8)

Using this relation between H_B and H, the numerator in the square root of α_1 is rewritten as

$$\frac{dH_B}{d\Delta_X} \approx \det \underline{\mathbf{D}} \frac{dH}{d\Delta_X} + H \frac{d\det \underline{\mathbf{D}}}{d\Delta_X}.$$
 (C9)

Note that α_1 has to be calculated at the EPD point and $H(\Delta_X, \omega)|_{\omega_{EPD}, X_{EPD}} = \det \underline{\mathbf{A}}(\Delta_X, \omega)|_{\omega_{EPD}, X_{EPD}} = 0$, so we simplify the above relation as

$$\frac{dH_B}{d\Delta_X}|_{\omega_{EPD}, X_{EPD}} \approx \det \mathbf{\underline{D}} \left| \chi_{EPD} \frac{dH}{d\Delta_X} \right|_{\omega_{EPD}, X_{EPD}}.$$
 (C10)

Analogously, the denominator in the square root of α_1 at the EPD point is found to be

$$\frac{d^{2}H_{B}}{d\omega^{2}}|_{\omega_{EPD}, X_{EPD}} \approx \det \underline{\mathbf{D}}|_{X_{EPD}} \frac{d^{2}H}{d\omega^{2}}|_{\omega_{EPD}, X_{EPD}}.$$
 (C11)

Therefore, we calculate the $d^2H_B/d\omega^2$ and $dH_B/d\Delta_X$ at the EPD point (ω_{EPD}, X_{EPD}) , leading to the approximation

for α₁ as

$$\alpha_{1} = \sqrt{-\frac{\frac{dH_{B}}{d\Delta_{X}}|_{\omega_{EPD}, X_{EPD}}}{\frac{1}{2!}\frac{d^{2}H_{B}}{d\omega^{2}}|_{\omega_{EPD}, X_{EPD}}}}}$$

$$\approx \sqrt{-\frac{\frac{dH}{d\Delta_{X}}|_{\omega_{EPD}, X_{EPD}}}{\frac{1}{2!}\frac{d^{2}H}{d\omega^{2}}|_{\omega_{EPD}, X_{EPD}}}}}.$$
(C12)

We conclude that α_1 found for the Puiseux series expansion of the ω -eigenvalues of $\underline{\mathbf{B}}(\Delta_X)$ is approximately the same as the coefficient used in the fractional power series expansion of the ω solutions of det $\mathbf{A}(\Delta_X, \omega) = 0$, demonstrating (19).

REFERENCES

- [1] B. van der Pol, "The nonlinear theory of electric oscillations," *Proc. IRE*, vol. 22, no. 9, pp. 1051–1086, Sep. 1934, doi: 10.1109/jr-proc.1934.226781.
- [2] B. Razavi, Design of Integrated Circuits for Optical Communications. New York, NY, USA: McGraw-Hill, 2002.
- [3] G. W. Pierce, "Piezoelectric crystal resonators and crystal oscillators applied to the precision calibration of wavemeters," in *Proc. Amer. Acad. Arts Sci.*, vol. 59, no. 4, 1923, pp. 81–106.
- [4] E. H. Colpitts, "Oscillation generator," U.S. Patent 1624 537A, Apr. 12, 1927.
- [5] R. E. Collin, Foundations for Microwave Engineering, 2nd ed. New York, NY, USA: Wiley, 2001.
- [6] A. Hajimiri, S. Limotyrakis, and T. Lee, "Jitter and phase noise in ring oscillators," *IEEE J. Solid-State Circuits*, vol. 34, no. 6, pp. 790–804, Jun. 1999, doi: 10.1109/4.766813.
- [7] T. Endo and S. Mori, "Mode analysis of a multimode ladder oscillator," IEEE Trans. Circuits Syst., vol. 23, no. 2, pp. 100–113, Feb. 1976, doi: 10.1109/tcs.1976.1084183.
- [8] A. Hajimiri and T. Lee, "A general theory of phase noise in electrical oscillators," *IEEE J. Solid-State Circuits*, vol. 33, no. 2, pp. 179–194, 1998, doi: 10.1109/4.658619.
- [9] H. Wu and A. Hajimiri, "Silicon-based distributed voltage-controlled oscillators," *IEEE J. Solid-State Circuits*, vol. 36, no. 3, pp. 493–502, Mar. 2001, doi: 10.1109/4.910488.
- [10] U. L. Rohde, A. K. Poddar, and G. Böck, *The Design of Modern Microwave Oscillators for Wireless Applications*. Hoboken, NJ, USA: Wiley, Jan. 2005, doi: 10.1002/0471727172.
- [11] B.-S. Song and T. Itoh, "Distributed bragg reflection dielectric wave-guide oscillators," *IEEE Trans. Microw. Theory Techn.*, vol. 27, no. 12, pp. 1019–1022, Dec. 1979, doi: 10.1109/tmtt.1979.1129783.
- [12] H.-A. Tanaka, A. Hasegawa, H. Mizuno, and T. Endo, "Synchronizability of distributed clock oscillators," *IEEE Trans. Circuits Syst. I, Fundam. Theory Appl.*, vol. 49, no. 9, pp. 1271–1278, Sep. 2002, doi: 10.1109/tcsi.2002.802361.
- [13] J. Lin and T. Itoh, "Two-dimensional quasi-optical power-combining arrays using strongly coupled oscillators," *IEEE Trans. Microw. Theory Techn.*, vol. 42, no. 4, pp. 734–741, Apr. 1994, doi: 10.1109/22.285088.
- [14] S. Nogi, J. Lin, and T. Itoh, "Mode analysis and stabilization of a spatial power combining array with strongly coupled oscillators," *IEEE Trans. Microw. Theory Techn.*, vol. 41, no. 10, pp. 1827–1837, Oct. 1993, doi: 10.1109/22.247929.
- [15] M. I. Vishik and L. A. Lyusternik, "The solution of some perturbation problems for matrices and selfadjoint or non-selfadjoint differential equations I," *Russian Math. Surv.*, vol. 15, no. 3, pp. 1–73, Jun. 1960, doi: 10.1070/rm1960v015n03abeh004092.
- [16] P. Lancaster, "On eigenvalues of matrices dependent on a parameter," *Numerische Mathematik*, vol. 6, no. 1, pp. 377–387, Dec. 1964, doi: 10.1007/bf01386087.
- [17] A. P. Seyranian, "Sensitivity analysis of multiple eigenvalues," J. Struct. Mechanics, vol. 21, no. 2, pp. 261–284, Jan. 1993, doi: 10.1080/08905459308905189.
- [18] T. Kato, Perturbation Theory for Linear Operators. New York, NY, USA: Springer-Verlag, 1966, doi: 10.1007/978-3-662-12678-3.

- [19] M. Berry, "Physics of nonhermitian degeneracies," *Czechoslovak J. Phys.*, vol. 54, no. 10, pp. 1039–1047, Oct. 2004, doi: 10.1023/b:cjop.0000044002.05657.04.
- [20] T. Stehmann, W. D. Heiss, and F. G. Scholtz, "Observation of exceptional points in electronic circuits," *J. Phys. A, Math. Gen.*, vol. 37, no. 31, 2004, Art. no. 7813, doi: 10.1088/0305-4470/37/31/012.
- [21] C. M. Bender, "Making sense of non-hermitian hamiltonians," Rep. Prog. Phys., vol. 70, no. 6, pp. 947–1018, May 2007, doi: 10.1088/0034-4885/70/6/r03.
- [22] H. Hodaei, M.-A. Miri, M. Heinrich, D. N. Christodoulides, and M. Khajavikhan, "Parity-time symmetric microring lasers," *Science*, vol. 346, no. 6212, pp. 975–978, Nov. 2014, doi: 10.1126/science.1258480.
- [23] L. Feng, Z. J. Wong, R.-M. Ma, Y. Wang, and X. Zhang, "Single-mode laser by parity-time symmetry breaking," *Science*, vol. 346, no. 6212, pp. 972–975, Nov. 2014, doi: 10.1126/science.1258479.
- [24] M. Sakhdari, M. Farhat, and P.-Y. Chen, "PT-symmetric metasurfaces: Wave manipulation and sensing using singular points," *New J. Phys.*, vol. 19, no. 6, Jun. 2017, Art. no. 065002, doi: 10.1088/1367-2630/aa6bb9.
- [25] P.-Y. Chen et al., "Generalized paritytime symmetry condition for enhanced sensor telemetry," Nature Electron., vol. 1, no. 5, pp. 297–304, May 2018, doi: 10.1038/s41928-018-0072-6.
- [26] C. E. Rüter, K. G. Makris, R. El-Ganainy, D. N. Christodoulides, M. Segev, and D. Kip, "Observation of paritytime symmetry in optics," *Nature Phys.*, vol. 6, no. 3, pp. 192–195, Jan. 2010, doi: 10.1038/nphys1515.
- [27] M. A. K. Othman and F. Capolino, "Theory of exceptional points of degeneracy in uniform coupled waveguides and balance of gain and loss," *IEEE Trans. Antennas Propag.*, vol. 65, no. 10, pp. 5289–5302, Oct. 2017, doi: 10.1109/TAP.2017.2738063.
- [28] M. A. K. Othman, V. Galdi, and F. Capolino, "Exceptional points of degeneracy and PT symmetry in photonic coupled chains of scatterers," *Phys. Rev. B*, vol. 95, no. 10, Mar. 2017, Art. no. 104305, doi: 10.1103/PhysRevB.95.104305.
- [29] A. F. Abdelshafy, M. A. K. Othman, D. Oshmarin, A. T. Almutawa, and F. Capolino, "Exceptional points of degeneracy in periodic coupled waveguides and the interplay of gain and radiation loss: Theoretical and experimental demonstration," *IEEE Trans. Antennas Propag.*, vol. 67, no. 11, pp. 6909–6923, Nov. 2019, doi: 10.1109/TAP.2019.2922778.
- [30] J. Schindler, A. Li, M. C. Zheng, F. M. Ellis, and T. Kottos, "Experimental study of active LRC circuits with PT symmetries," *Phys. Rev. A*, vol. 84, no. 4, 2011, Art. no. 040101.
- [31] A. Nikzamir, K. Rouhi, A. Figotin, and F. Capolino, "Demonstration of exceptional points of degeneracy in gyrator-based circuit for highsensitivity applications," 2021, arXiv:2107.00639.
- [32] K. Rouhi, A. Nikzamir, A. Figotin, and F. Capolino, "Exceptional point in a degenerate system made of a gyrator and two unstable resonators," *Phys. Rev. A*, vol. 105, no. 3, Mar. 2022, Art. no. 032214, doi: 10.1103/physreva.105.032214.
- [33] A. Figotin and I. Vitebskiy, "Gigantic transmission bandedge resonance in periodic stacks of anisotropic layers," *Phys. Rev. E*, vol. 72, no. 3, Sep. 2005, Art. no. 036619, doi: 10.1103/physreve.72.036619.
- [34] M. A. K. Othman and F. Capolino, "Demonstration of a degenerate band edge in periodically-loaded circular waveguides," *IEEE Microw. Wireless Compon. Lett.*, vol. 25, no. 11, pp. 700–702, Nov. 2015, doi: 10.1109/lmwc.2015.2479845.

- [35] J. T. Sloan, M. A. K. Othman, and F. Capolino, "Theory of double ladder lumped circuits with degenerate band edge," *IEEE Trans. Circuits Syst. I, Reg. Papers*, vol. 65, no. 1, pp. 3–13, Jan. 2018, doi: 10.1109/TCSI.2017.2690971.
- [36] T. Mealy and F. Capolino, "General conditions to realize exceptional points of degeneracy in two uniform coupled transmission lines," *IEEE Trans. Microw. Theory Techn.*, vol. 68, no. 8, pp. 3342–3354, Aug. 2020, doi: 10.1109/TMTT.2020.2999498.
- [37] A. F. Abdelshafy, T. Mealy, E. Hafezi, A. Nikzamir, and F. Capolino, "Exceptional degeneracy in a waveguide periodically loaded with discrete gain and radiation loss elements," *Appl. Phys. Lett.*, vol. 118, no. 22, May 2021, Art. no. 224102, doi: 10.1063/5.0051238.
- [38] M. Y. Nada, M. A. K. Othman, and F. Capolino, "Theory of coupled resonator optical waveguides exhibiting high-order exceptional points of degeneracy," *Phys. Rev. B*, vol. 96, no. 18, Nov. 2017, Art. no. 184304, doi: 10.1103/PhysRevB.96.184304.
- [39] D. Oshmarin et al., "New oscillator concept based on band edge degeneracy in lumped double-ladder circuits," *IET Circuits, Devices Syst.*, vol. 13, no. 7, pp. 950–957, Jul. 2019, doi: 10.1049/iet-cds.2018.5048.
- [40] H. Kazemi, M. Y. Nada, T. Mealy, A. F. Abdelshafy, and F. Capolino, "Exceptional points of degeneracy induced by linear time-periodic variation," *Phys. Rev. Appl.*, vol. 11, Jan. 2019, Art. no. 014007, doi: 10.1103/PhysRevApplied.11.014007.
- [41] H. Kazemi, M. Y. Nada, A. Nikzamir, F. Maddaleno, and F. Capolino, "Experimental demonstration of exceptional points of degeneracy in linear time periodic systems and exceptional sensitivity," *J. Appl. Phys.*, vol. 131, no. 14, Apr. 2022, Art. no. 144502, doi: 10.1063/5.0084849.
- [42] H. Kazemi et al., "Ultra-sensitive radio frequency biosensor at an exceptional point of degeneracy induced by time modulation," *IEEE Sensors J.*, vol. 21, no. 6, pp. 7250–7259, Mar. 2021, doi: 10.1109/JSEN.2020.3047886.
- [43] D. Oshmarin, A. F. Abdelshafy, A. Nikzamir, M. M. Green, and F. Capolino, "Experimental demonstration of a new oscillator concept based on degenerate band edge in microstrip circuit," 2021, arXiv:2109.07002.
- [44] D. M. Pozar, Microwave Engineering, 4th ed. New York, NY, USA: Wiley, 2009.
- [45] S. J. Orfanidis, "Electromagnetic waves and antennas," Rutgers University New Brunswick, NJ, USA, 2002.
- [46] K. Scharnhorst, "Angles in complex vector spaces," Acta Applicandae Mathematicae, vol. 69, no. 1, pp. 95–103, 2001, doi: 10.1023/a:1012692601098.
- [47] A. Galántai and C. J. Hegedüs, "Jordan's principal angles in complex vector spaces," *Numer. Linear Algebra Appl.*, vol. 13, no. 7, pp. 589–598, 2006, doi: 10.1002/nla.491.
- [48] J. Wiersig, "Sensors operating at exceptional points: General theory," *Phys. Rev. A*, vol. 93, no. 3, Mar. 2016, Art. no. 033809, doi: 10.1103/PhysRevA.93.033809.
- [49] J. Moro, J. V. Burke, and M. L. Overton, "On the Lidskii-Vishik-Lyusternik perturbation theory for eigenvalues of matrices with arbitrary Jordan structure," SIAM J. Matrix Anal. Appl., vol. 18, no. 4, pp. 793–817, Oct. 1997, doi: 10.1137/s0895479895294666.
- [50] A. Welters, "On explicit recursive formulas in the spectral perturbation analysis of a Jordan block," SIAM J. Matrix Anal. Appl., vol. 32, no. 1, pp. 1–22, Jan. 2011, doi: 10.1137/090761215.